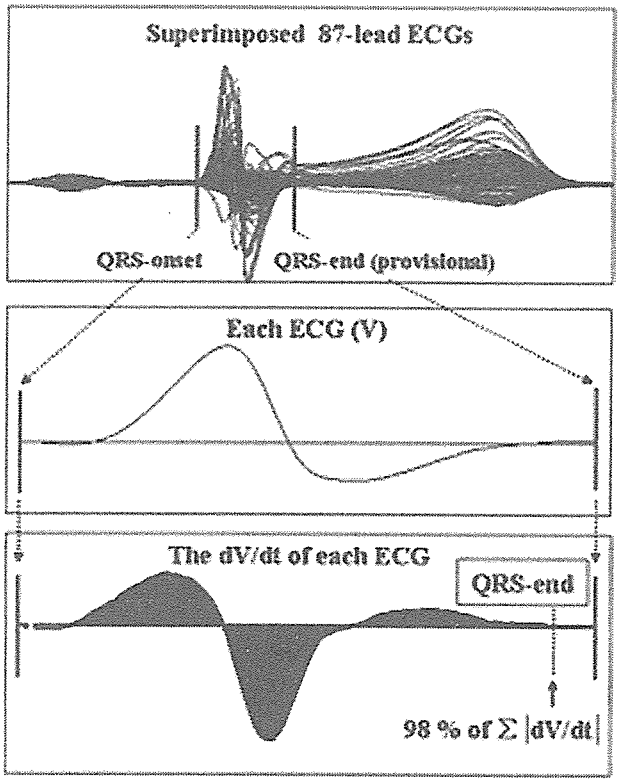

Figure 3. *The algorithm for determination of the end of QRS (QRS-end) in each electrocardiogram. With superimposed 87-leads ECG, the onset of QRS was first determined by detecting the earliest deflection, and then the QRS-end was provisionally determined by visual inspection of all 87-leads. Thereafter, the first derivative of QRS voltage (dV/dt) and its algebraic summation of the absolute value indicated by the area colored in black were computed in each lead. The QRS-end was defined as the time-point where the cumulative area from the QRS-onset reached 98% of the total area.*

by using one-way ANOVA, followed by Scheffe's test. A P value < 0.05 was considered significant.

Results

Figure 4A–C shows the 87-leads ECG (a) and 6-leads ECG, reflecting potentials of the RVOT region (b) in a representative patient with Brugada syndrome.

ECG Parameters in the RVOT Region and the Other Region Before and After Pharmacological Interventions

Figure 5A–C depicts composite data of each ECG parameter of 6-leads and 81-leads before and after pharmacological interventions in the 28 patients with Brugada syndrome.

The ST-segment was elevated under baseline condition only in 6-leads, and the baseline ST20 was significantly higher in 6-leads than in 81-leads (0.22 ± 0.10 mV vs 0.02 ± 0.02 mV; $P < 0.0005$) (Fig. 5A). In 6-leads reflecting the RVOT potentials, the ST20 was decreased by isoproterenol (0.11 ± 0.09 mV; $P < 0.0005$ vs baseline) and augmented by pilsicainide (0.33 ± 0.11 mV; $P < 0.0005$ vs baseline) significantly (Fig. 5A, left panel). In contrast, the ST20 was not changed in 81-leads after pharmacological interventions (Isoproterenol: 0.01 ± 0.01 mV; Pilsicainide: 0.01 ± 0.02 mV; P = N.S. vs baseline) (Fig. 5A, right panel).

The baseline RTc was significantly longer in 6-leads than in 81-leads (325 ± 46 ms vs 302 ± 24 ms; $P < 0.05$) (Fig. 5B). Isoproterenol infusion slightly prolonged the RTc in 81-leads (327 ± 28 ms; $P < 0.05$ vs baseline) (Fig. 5B, right panel). The RTc was further prolonged by pilsicainide only in 6-leads (354 ± 42 ms; $P < 0.005$ vs baseline) (Fig. 5B, left panel), while it was not changed by pilsicainide in 81-leads (309 ± 23 ms) (Fig. 5B, right panel).

The baseline QRS duration was slightly prolonged both in 6-leads and 81-leads, but not different between the two regions (107 ± 14 ms vs 104 ± 14 ms; P = N.S.) (Fig. 5C). In both regions, the QRS duration was not changed by isoproterenol (6-leads: 106 ± 14 ms; 81-leads: 103 ± 14 ms; P = N.S. vs baseline, respectively), but further increased by pilsicainide (6-leads: 125 ± 18 ms; 81-leads: 121 ± 18 ms; $P < 0.0005$ vs baseline, respectively). However, the prolongation of the QRS duration with pilsicainide was homogeneous between the two regions.

Comparison of Changes (Δ) of ECG Parameters with Pharmacological Intervention Between the RVOT Region and the Other Region

Figure 6A and B illustrates comparison of changes (Δ) of each ECG parameter with isoproterenol and pilsicainide between 6-leads and 81-leads in the 28 patients with Brugada syndrome.

During isoproterenol infusion, the ΔST20 was significantly larger in 6-leads than in 81-leads (-0.12 ± 0.09 mV vs -0.01 ± 0.01 mV; $P < 0.0005$). Both ΔRTc and ΔQRS duration were not different between the two regions (ΔRTc: 6-leads, 19 ± 39 ms vs 81-leads, 25 ± 24 ms; ΔQRS duration: 6-leads, -1 ± 3 ms vs 81-leads, -1 ± 3 ms; P = N.S., respectively).

After pilsicainide injection, the ΔST20 was significantly larger in 6-leads than in 81-leads (0.10 ± 0.05 mV vs 0.00 ± 0.01 mV; $P < 0.0005$). The ΔRTc was also significantly larger in 6-leads than in 81-leads (28 ± 38 ms vs 7 ± 17 ms; $P < 0.05$). In contrast, the ΔQRS duration was not different between the two regions (6-leads: 18 ± 12 ms vs 81-leads: 17 ± 9 ms; P = N.S.).

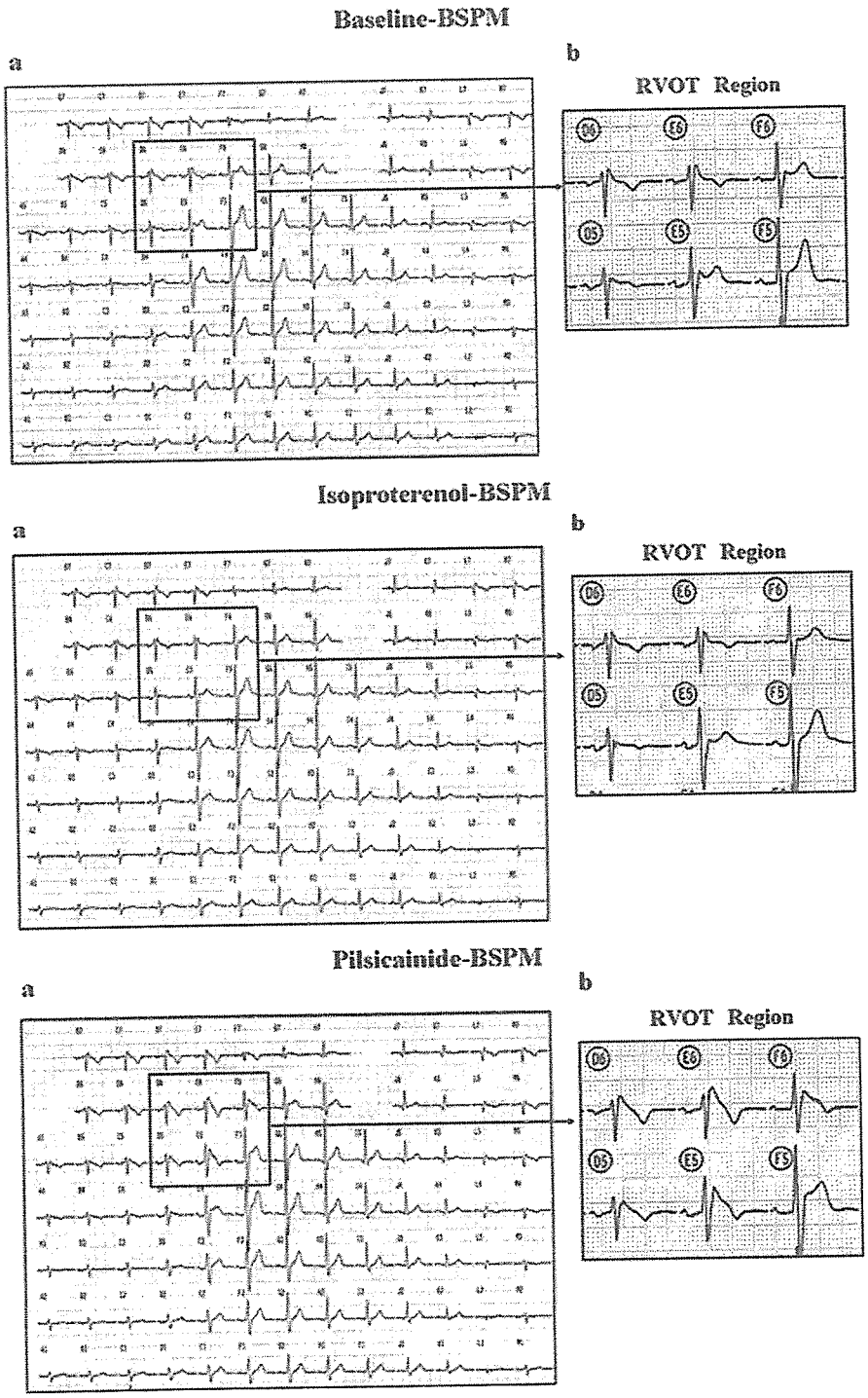

Figure 4. *Eighty-seven-leads electrocardiogram (ECG) (a), and 6-leads ECG (D-F, 5-6) reflecting potentials of the right ventricular outflow tract (RVOT) (b) in a representative patient with Brugada syndrome. (A) Baseline condition. The coved- or saddleback-type ST-segment elevation was seen only in 6-leads, and the mean ST20 was higher in 6-leads (0.17 ± 0.06 mV) than in 81-leads (0.00 ± 0.03 mV). The mean corrected recovery time (RTc) was slightly longer in 6-leads (320 ± 57 ms) than in 81-leads (309 ± 38 ms). The mean QRS duration was slightly prolonged both in 6-leads (109 ± 5 ms) and in 81-leads (102 ± 7 ms), but no major difference was observed between the two regions. (B) Isoproterenol infusion. The ST-segment elevation was normalized in 6-leads (0.07 ± 0.02 mV), but not changed in 81-leads (0.00 ± 0.01 mV). The mean RTc was slightly prolonged with isoproterenol both in 6-leads (346 ± 42 ms) and 81-leads (332 ± 68 ms). The mean QRS duration was not changed with isoproterenol in either 6-leads (102 ± 5 ms) or 81-leads (100 ± 5 ms). (C) Pilsicainide injection. The ST-segment elevation was dramatically augmented only in 6-leads (0.31 ± 0.11 mV), but not changed in 81-leads (0.01 ± 0.04 mV). Pilsicainide prolonged the mean RTc in only 6-leads (336 ± 53 ms), but not in 81-leads (293 ± 42 ms). On the other hand, the mean QRS duration was increased by pilsicainide homogeneously in 6-leads (121 ± 4 ms) and in 81-leads (116 ± 5 ms).*

ECG Parameters Between Patients with *SCN5A* Mutation and Those without *SCN5A* Mutation

The ECG parameters and their changes were compared between 4 patients with *SCN5A* mutation and 24 patients without *SCN5A* mutation. Although the baseline QRS duration was not different between the two groups, the QRS duration after pilsicainide was significantly longer in the *SCN5A* positive patients than in the *SCN5A* negative patients both in 6-leads (138 ± 22 ms vs 123 ± 17 ms; $P < 0.005$) and in 81-leads (134 ± 20 ms vs 119 ± 17 ms; $P < 0.005$).

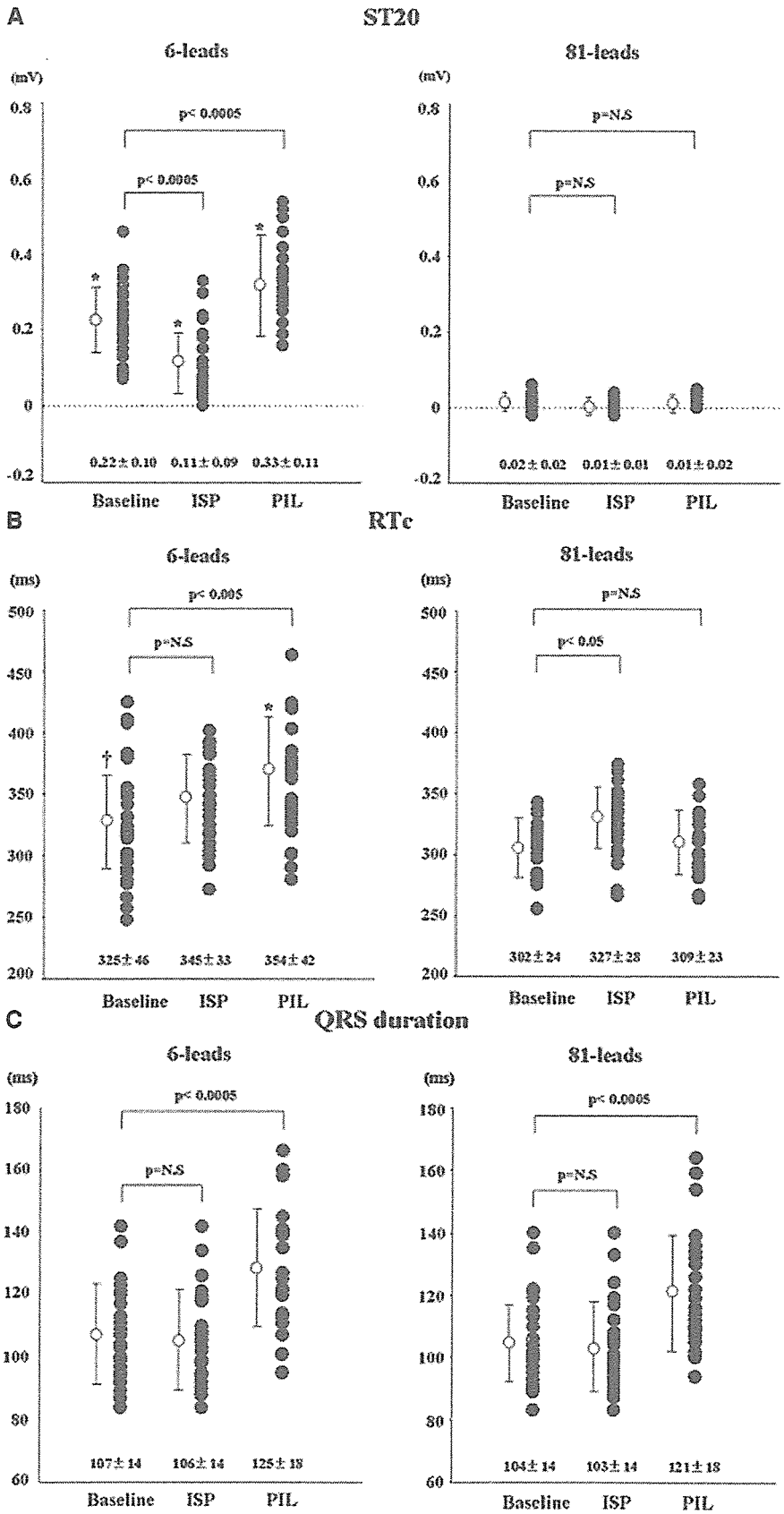

Figure 5. *Composite data of ECG parameters of 6-leads (RVOT region) and 81-leads (Other region) under baseline condition, during isoproterenol infusion (ISP), and after pilsicainide injection (PIL) in the 28 patients with Brugada syndrome. (A) The baseline ST20 was significantly higher in 6-leads than in 81-leads. The ST20 was decreased by isoproterenol and augmented by pilsicainide significantly in 6-leads, while it was not changed in 81-leads. (B) The baseline corrected recovery time (RTc) was longer in 6-leads than in 81-leads. The RTc was significantly prolonged by pilsicainide in only 6-leads. Isoproterenol infusion slightly but significantly prolonged the RTc in 81-leads. (C) The baseline QRS duration was slightly prolonged both in 6-leads and 81-leads. The QRS duration was not changed by isoproterenol, but further increased homogeneously by pilsicainide in both regions. *P < 0.0005, †P < 0.05 versus 81-leads.*

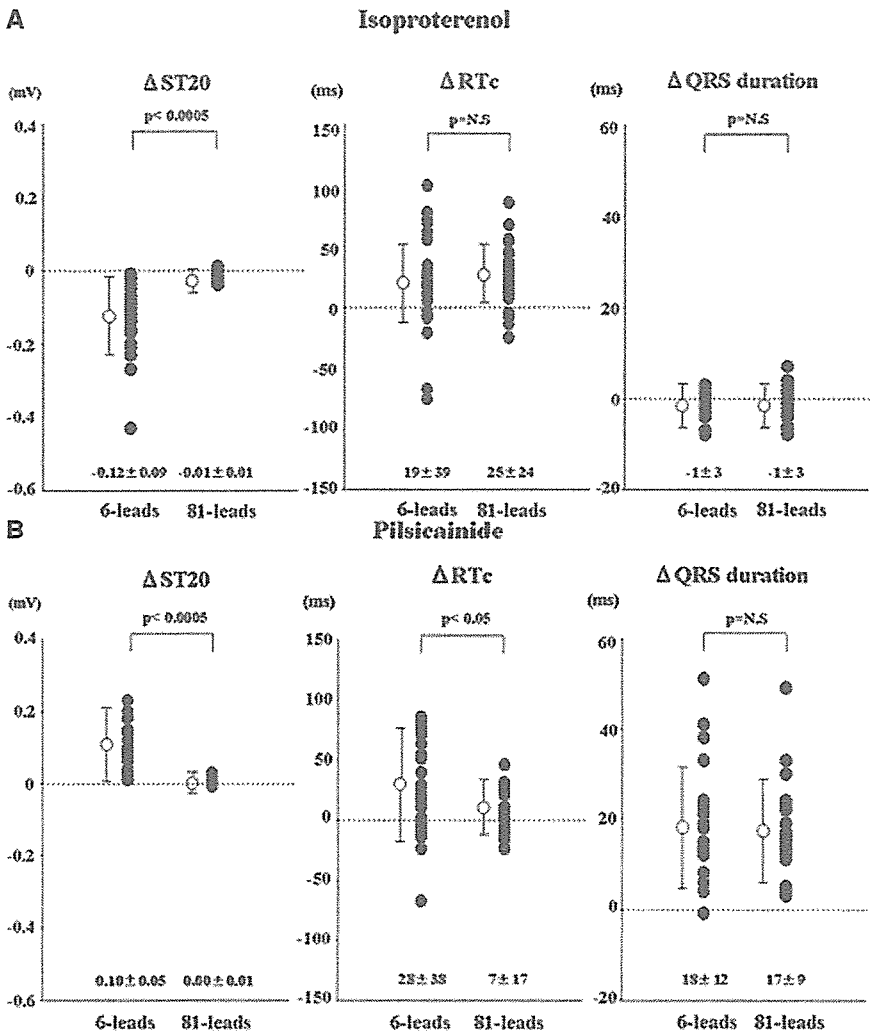

Figure 6. *Comparison of changes (Δ) of ECG parameters with pharmacological interventions between 6-leads (RVOT region) and 81-leads (Other region) in the 28 patients with Brugada syndrome. (A) Isoproterenol infusion. The ΔST20 was significantly larger in 6-leads than in 81-leads, while both ΔRTc and ΔQRS duration were not different between the two regions. (B) Pilsicainide injection. The ΔST20 and the ΔRTc were significantly larger in 6-leads than in 81-leads, while the ΔQRS duration was not different between the two regions.*

The ΔQRS duration with pilsicainide was also significantly larger in the *SCN5A* positive patients than in the *SCN5A* negative patients both in 6-leads (36 ± 16 ms vs 15 ± 8 ms; $P < 0.005$) and in 81-leads (31 ± 15 ms vs 15 ± 6 ms; $P < 0.005$). No significant differences were observed in other ECG parameters and their changes between 4 patients with *SCN5A* mutation and 24 patients without *SCN5A* mutation.

ECG Parameters Between Patients with Spontaneous Type 1 ECG and Those with Sodium Channel Blocker-Induced Type 1 ECG

Since it is generally accepted that Brugada patients with spontaneous Type 1 ECG are at higher risk of cardiac events than those with sodium channel blocker-induced Type 1 ECG, we compared the ECG parameters and the change of the ECG parameters between 17 patients with spontaneous Type 1 ECG and 11 patients with sodium channel blocker-induced Type 1 ECG. There were no significant differences in the ECG parameters between the two groups, except for the ST20 under baseline condition and after isoproterenol and pilsicainide. The changes of each ECG parameter by pharmacological interventions showed similar tendency between the two groups (data not shown).

Discussion

The major findings of the present study were: (1) the ST-segment elevation and RTc prolongation were localized and modulated by pharmacological interventions only in the region of RVOT, and (2) the slight prolongation of QRS duration at baseline and its further increase by a sodium channel blocker, pilsicainide, were observed homogeneously throughout the ventricular wall.

Transmural Electrical Heterogeneity of Repolarization Localized in the RVOT

The ST-segment elevation in the right precordial leads in patients with Brugada syndrome

is thought to result from transmural heterogeneity in action potential (AP) configuration in the RVOT.[15,16] Experimental data using arterially perfused right ventricular wedge preparations have suggested that prominent transient outward current (I_{to})-mediated AP notch and a loss of AP dome in epicardium, but not in endocardium, give rise to a transmural voltage gradient, resulting in ST-segment elevation.[15] Since the maintenance of the epicardial AP dome is determined by the balance of currents active at the end of phase 1 of the AP (principally I_{to} and L-type calcium current (I_{Ca-L})), any interventions that increase outward currents (e.g., I_{to}, slow and fast activating components of delayed rectifier potassium current (I_{Ks}, I_{Kr})) or decrease inward currents (e.g., I_{Ca-L}, fast I_{Na}) can accentuate ST-segment elevation.[16] Among these interventions, class IC sodium channel blockers, such as pilsicainide, most effectively amplify or unmask ST-segment elevation secondary to their strong effect to block fast I_{Na}.[24–26] On the other hand, isoproterenol, a β-adrenergic stimulant, strongly augments I_{Ca-L}, and therefore, attenuates ST-segment elevation.[27]

Several previous studies have examined the spatial distribution of depolarization and repolarization abnormalities by using BSPM system.[28–31] In the present study, we evaluated the ST-segment amplitude (ST20) and the RTc as repolarization parameters. Because the maximum dV/dt point of T wave in the ECG is shown to correspond to the minimum dV/dt point of the epicardial AP, the RT is approximately the sum of the activation time and the AP duration at 90% repolarization in the epicardial cell.[32]

The effect of isoproterenol to normalize the ST-segment elevation in the RVOT region is thought to be as a result of decreased transmural voltage gradient due to decreased phase 1 notch in the epicardial AP. On the other hand, pilsicainide induced the coved-type ST-segment elevation, the terminal negative T wave, and the prolongation of RT only in the RVOT region. These changes in the electrocardiographic phenotype are probably due to the accentuated phase 1 notch and a greater prolongation of the epicardial AP duration or phase 2 reentry-induced second epicardial AP, resulting in reversed transmural voltage gradient between the epicardial and the endocardial APs.

Sodium Channel Defect and Depolarization Abnormality

The first mutation linked to Brugada syndrome was identified in *SCN5A*, the gene encoding α-subunit of the sodium channel; and functional studies of *SCN5A* mutations responsible for the Brugada phenotype have demonstrated the "loss of function" of I_{Na} by several mechanisms.[17]

Mild conduction abnormalities, such as widening of P wave, prolongation of QRS duration, PQ interval and HV interval, and higher incidence of right bundle-branch block, have been described in patients with Brugada syndrome.[8,12] Signal-averaged ECG recordings have demonstrated late potentials in approximately two-thirds of Brugada patients.[5] Some *SCN5A* mutations responsible for Brugada phenotype are reported to be associated with more severe conduction disease (i.e., depolarization abnormalities). Moreover, recent histological studies in patients with Brugada syndrome have shown the presence of concealed structural abnormalities and conduction slowing in the RVOT area.[33,34]

We recently conducted a high-resolution optical mapping in an experimental Brugada model employing a canine right ventricular wedge preparation, which allowed a detailed measurement of cellular repolarization and depolarization in the epicardial and endocardial surfaces.[35] Our data suggested that the initiating ventricular premature beats were caused by phase 2 reentry originated from the epicardial area with a steep gradient of ventricular repolarization time due to heterogeneous loss of the AP dome. In contrast, wave-break appeared at sites of delayed epicardial conduction during the first few reentrant waves, which was closely associated with VF susceptibility, suggesting that conduction abnormalities contribute to the maintenance of VF under the Brugada condition.

It is still unclear whether depolarization abnormalities are localized in the region of RVOT or distributed homogeneously in the whole ventricle. We measured the QRS duration from all 87-leads BSPM as a depolarization parameter by using our original algorithm in the present study. Mild prolongation of the QRS duration under baseline condition and its further prolongation by a sodium channel blocker were observed homogeneously between the RVOT region and the other region. Our data suggest that depolarization abnormality is distributed homogeneously throughout the ventricle, probably due to sodium channel dysfunction.

Study Limitations

First limitation of the present study is that the electrocardiographic measurements were made in the body surface region, but not in the ventricular wall directly. There is no one-to-one correspondence between the measurements from the body surface and those from the ventricular wall. This is because every electrode on the body surface records potentials that are generated by activity in the entire heart, although weighted by proximity.

Second, we measured RT but not QT interval as a repolarization parameter in the present study,

because the QT interval is difficult to measure semi-automatically. Moreover, the end of the QT interval is expected to coincide with full repolarization of several cell types, depending on the morphology of the T wave. In the case of saddleback-type ST elevation and coved-type ST elevation without negative T wave, repolarization of the epicardial AP is earlier than that of the endocardial AP, and thus repolarization of subendocardial cell coincides with the end of the QT interval. On the other hand, in the case of coved-type ST elevation with negative T wave, repolarization of the epicardial AP is later than that of the endocardial AP, and thus repolarization of epicardial cell coincides with the end of the QT interval. As a depolarization parameter, we examined the QRS duration, but not the ventricular activation time (VAT) defined as the interval between QRS-onset and minimum dV/dt point of the QRS. This was because the accentuated J-point and ST-segment elevation are superimposed on the late r' wave in the right precordial leads in patients with Brugada syndrome; thus the VAT seems to be overestimated in the RVOT region.

Acknowledgments: Dr. W. Shimizu was supported by the Hoansha Research Foundation; Japan Research Foundation for Clinical Pharmacology; Ministry of Education, Culture, Sports, Science and Technology Leading Project for Biosimulation; and health sciences research grants (H18—Research on Human Genome, Tissue Engineering) from the Ministry of Health, Labour and Welfare, Japan.

References

1. Brugada P, Brugada J. Right bundle branch block, persistent ST segment elevation and sudden cardiac death: A distinct clinical and electrocardiographic syndrome: A multicenter report. J Am Coll Cardiol 1992; 20:1391–1396.
2. Brugada J, Brugada P. Further characterization of the syndrome of right bundle branch block, ST segment elevation, and sudden cardiac death. J Cardiovasc Electrophysiol 1997; 8:325–331.
3. Brugada J, Brugada R, Brugada P. Right bundle-branch block and ST-segment elevation in V1 through V3. A marker for sudden death in patients without demonstrable structural heart disease. Circulation 1998; 97:457–460.
4. Wilde AA, Antzelevitch C, Borggrefe M, et al. Study group on the molecular basis of arrhythmias of the European society of cardiology. Proposed diagnostic criteria for the Brugada syndrome: Consensus report. Circulation 2002; 106:2514–2519.
5. Antzelevitch C, Brugada P, Borggrefe M, et al. Brugada syndrome: Report of the second consensus conference: Endorsed by the Heart Rhythm Society and the European Heart Rhythm Association. Circulation 2005; 111:659–670.
6. Antzelevitch C, Brugada P, Borggrefe M, et al. Brugada syndrome: Report of the second consensus conference. Heart Rhythm 2005; 2:429–440.
7. Priori SG, Napolitano C, Gasparini M, et al. Natural history of Brugada syndrome: Insights for risk stratification and management. Circulation 2002; 105:1342–1347.
8. Priori SG, Napolitano C, Memmi M, et al. Clinical and genetic heterogeneity of right bundle branch block and ST-segment elevation syndrome: A prospective evaluation of 52 families. Circulation 2000; 102:2509–2515.
9. Shimizu W, Aiba T, Kamakura S. Mechanisms of diseases: Current understanding and future challenges in Brugada syndrome. Nat Clin Pract Cardiovasc Med 2005; 2:408–414.
10. Nademanee K, Veerakul G, Nimmannit S, et al. Arrhythmogenic marker for the sudden unexplained death syndrome in Thai men. Circulation 1997; 96:2595–2600.
11. Pitzalis MV, Anaclerio M, Iacoviello M, et al. QT-interval prolongation in right precordial leads: An additional electrocardiographic hallmark of Brugada syndrome. J Am Coll Cardiol 2003; 42:1632–1637.
12. Smits JP, Eckardt L, Probst V, et al. Genotype-phenotype relationship in Brugada syndrome: Electrocardiographic features differentiate SCN5A-related patients from non-SCN5A-related patients. J Am Coll Cardiol 2002; 40:350–356.
13. Nagase S, Kusano KF, Morita H, et al. Epicardial electrogram at the right ventricular outflow tract in patients with the Brugada syndrome: Using the epicardial leads. J Am Coll Cardiol 2002; 39:1992–1995.
14. Antzelevitch C. Late potentials and the Brugada syndrome. J Am Coll Cardiol 2002; 39:1996–1999.
15. Yan GX, Antzelevitch C. Cellular basis for the Brugada syndrome and other mechanisms of arrhythmogenesis associated with ST-segment elevation. Circulation 1999; 100:1660–1666.
16. Antzelevitch C. The Brugada syndrome: Ionic basis and arrhythmia mechanisms. J Cardiovasc Electrophysiol 2001; 12:268–272.
17. Meregalli PG, Wilde AA, Tan HL. Pathophysiological mechanisms of Brugada syndrome: Depolarization disorder, repolarization disorder, or more? Cardiovasc Res 2005; 67:367–378.
18. Roden DM, Wilde AA. Drug-induced J point elevation: A marker for genetic risk of sudden death or ECG curiosity? J Cardiovasc Electrophysiol 1999; 10:219–223.
19. Shimizu W, Kamakura S, Kurita T, Suyama K, Aihara N, Shimomura K. Influence of epinephrine, propranolol, and atrial pacing on spatial distribution of recovery time measured by body surface mapping in congenital long QT syndrome. J Cardiovasc Electrophysiol 1997; 8:1102–1114.
20. Shimizu W, Matsuo K, Takagi M, et al. Body surface distribution and response to drugs of ST segment elevation in Brugada syndrome: Clinical implication of eighty-seven-lead body surface potential mapping and its application to twelve-lead electrocardiograms. J Cardiovasc Electrophysiol 2000; 11:396–404.
21. Kamakura S, Shimizu W, Matsuo K, et al. Localization of the optimal ablation site of idiopathic ventricular tachycardia from right and left ventricular outflow tract by body surface electrocardiogram. Circulation 1998; 98:1525–1533.
22. Tahara N, Takaki H, Taguchi A, et al. Exercise-induced QRS prolongation in patients with mild coronary artery disease: Computer analysis of the digitized multilead ECGs. J Electrocardiol 1999; 32:206–211.
23. Sakuragi S, Takaki H, Taguchi A, et al. Diagnostic value of the recovery time-course of ST slope on exercise in discriminating false-from true-positive ST-segment depressions. Circ J 2004; 68:915–922.
24. Krishnan SC, Josephson ME. ST segment elevation induced by class IC antiarrhythmic agents: Underlying electrophysiologic mechanisms and insights into drug-induced proarrhythmia. J Cardiovasc Electrophysiol 1998; 9:1167–1172.
25. Fujiki A, Usui M, Nagasawa H, Mizumaki K, Hayashi H, Inoue H. ST segment elevation in the right precordial leads induced with class IC antiarrhythmic drug: Insight into the mechanism of Brugada syndrome. J Cardiovasc Electrophysiol 1999; 10:214–218.
26. Shimizu W, Antzelevitch C, Suyama K, et al. Effect of sodium channel blockers on ST segment, QRS duration, and corrected QT interval in patients with Brugada syndrome. J Cardiovasc Electrophysiol 2000; 11:1320–1329.
27. Miyazaki T, Mitamura H, Miyoshi S, Soejima K, Aizawa Y, Ogawa S. Autonomic and antiarrhythmic drug modulation of ST segment elevation in patients with Brugada syndrome. J Am Coll Cardiol 1996; 27:1061–1070.
28. Eckardt L, Bruns HJ, Paul M, et al. Body surface area of ST elevation and the presence of late potentials correlate to the inducibility of ventricular tachyarrhythmias in Brugada syndrome. J Cardiovasc Electrophysiol 2002; 13:742–749.
29. Bruns HJ, Eckardt L, Vahlhaus C, et al. Body surface potential mapping in patients with Brugada syndrome: Right precordial ST segment variations and reverse changes in left precordial leads. Cardiovasc Res 2002; 54:58–66.
30. Hisamatsu K, Kusano KF, Morita H, et al. Relationships between depolarization abnormality and repolarization and abnormality

in patients with Brugada syndrome: Using bodysurface signal-averaged electrocardiography and body surface maps. J Cardiovasc Electrophysiol 2004; 15:870–876.
31. Izumida N, Asano Y, Doi S, et al. Changes in body surface potential distributions induced by isoproterenol and Na channel blockers in patients with the Brugada syndrome. Int J Cardiol 2004; 95:261–268.
32. Haws CW, Lux RL. Correlation between in vivo transmembrane action potential durations and activation-recovery intervals from electrograms: Effects of interventions that alter repolarization time. Circulation 1990; 81:281–288.
33. Coronel R, Casini S, Koopmann TT, et al. Right ventricular fibrosis and conduction delay in a patient with clinical signs of Brugada syndrome: A combined electrophysiological, genetic, histopathologic, and computational study. Circulation 2005; 112:2769–2777.
34. Frustaci A, Priori SG, Pieroni M, et al. Cardiac histological substrate in patients with clinical phenotype of Brugada syndrome. Circulation 2005; 112:3680–3687.
35. Aiba T, Shimizu W, Hidaka I, et al. Cellular basis for trigger and maintenance of ventricular fibrillation in the Brugada syndrome model: High resolution optical mapping study. J Am Coll Cardiol 2006; 47:2074–2085.

Summary: An amphiphilic poly(*N*-propargylamide) with galactose and lauryloyl groups was synthesized by copolymerization of the corresponding *N*-propargylamide monomers using a Rh catalyst. The obtained copolymer formed a one-handed helical conformation and molecular aggregates in water. The observations by fluorescence microscopy in a cell culture experiment in the presence of dye-labeled copolymer indicated that the copolymer was incorporated into the cells.

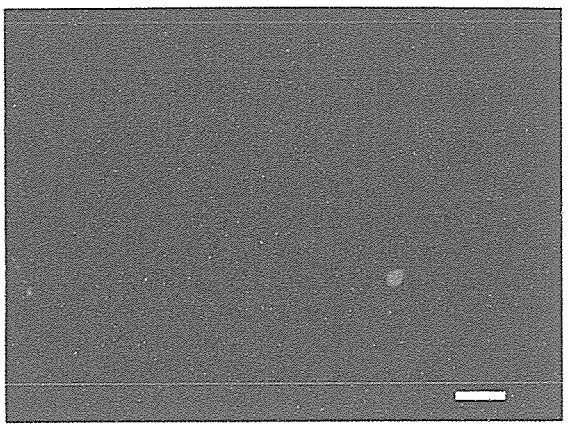

Localization of rhodamine B-labeled copolymer **8** in human aortic endothelial cells (fluorescence image).

Amphiphilic Poly(*N*-propargylamide) with Galactose and Lauryloyl Groups: Synthesis and Properties

Masakazu Suenaga,[1] *Yoshiro Kaneko,*[1] *Jun-ichi Kadokawa,**[1] *Takehiro Nishikawa,*[2] *Hidezo Mori,*[2] *Masayoshi Tabata*[3]

[1]Department of Nanostructured and Advanced Materials, Graduate School of Science and Engineering, Kagoshima 890-0065, Japan
Fax: +81-99-285-3253; E-mail: kadokawa@eng.kagoshima-u.ac.jp
[2]National Cardiovascular Center, Suita, Osaka 565-8565, Japan
[3]Department of Molecular Chemistry, Graduate School of Engineering, Hokkaido University, Sapporo 060-8628, Japan

Received: July 19, 2006; Accepted: October 10, 2006; DOI: 10.1002/mabi.200600228

Keywords: amphiphiles; conjugated polymers; copolymerization; dynamic light scattering; nanoparticles; polyacetylenes

Introduction

Synthesis of polymers having sugar residues, so-called glycopolymers, has been widely investigated to seek biological applications because of their versatile functions.[1] It has been demonstrated that these glycopolymers can bind specifically to carbohydrate-recognition proteins, toxins, viruses, and cells, and, thus, these polymers can be utilized as cell culture substrates with specific cell recognition sites, as well as in targeting drug delivery systems.[2] The clustered saccharide ligands conjugated to the polymeric main chains are involved in these specific recognition processes. Most of the previously prepared glycopolymers have been based on a flexible polymer backbone, such as polystyrene and polyacrylamide.[3,4] This flexible nature of the glycopolymers causes the disordered orientation of the sugar residues in the glycopolymers. Regular orientation of the sugar residues is necessary for efficient interaction between the glycopolymers and receptor molecules. In this sense, the spatially regulated orientation of the sugar residues should be realized by attaching the sugar residues to a polymer backbone with a rigid conformation. The sugar residues attached to the rigid polymer backbone may give rise to the ordered orientation that can improve the molecular recognition of sugar residues by specific cell receptors. This is because the spatial regulation of the sugar residues is significant in molecular recognition as well as the chemical structure of the sugar molecules.[5]

From the above viewpoints, rigid glycopolymers with π-conjugated polymer backbones would be a novel type of bio-inspired polymers, which could exhibit multiple valence states and interact specifically and firmly with targets such as cell surface receptors and biomacromolecules. In some previous works, rigid glycopolymers having various π-conjugated main chains, such as polythiophene,[6] poly(*p*-phenylene ethynylene),[7] polyisocyanide,[8] polyaniline,[9] poly(*p*-phenylene vinylene),[10] and poly(phenylacetylene), have already been synthesized.[11] In the series of these studies, we reported the synthesis of poly(*N*-propargylamide) (**2**) with sugar residues. It contained a *cis*-polyacetylene main chain and was obtained by the rhodium-catalyzed polymerization of a *N*-propargylamide monomer (**1**) that had a galactose residue (Scheme 1).[12] Since polymerizations of the *N*-propargylamide monomers having various substituted groups using Rh catalyst have been widely reported to produce the corresponding poly(*N*-propargylamide) derivatives with *cis*-isomers,[13] we also investigated the copolymerization of **1** with *N*-propargylamide derivative **3** having a hexanoyl group to produce the amphiphilic glycopolymer **4**, as shown in Scheme 1. We tested the solubility of copolymer **4** in various solvents to confirm whether the copolymer exhibits an amphiphilic property. Although the homopolymer **2** is insoluble in common organic solvents, the copolymer **4** can be dissolved in some polar organic solvents, such as dimethyl sulfoxide (DMSO) and *N,N*-dimethylformamide (DMF), as well as in aqueous medium. However, the copolymer still exhibits a hydrophilic nature rather than an amphiphilic nature. We assumed that insufficient amphiphilicity of copolymer **4** could be attributed to poor hydrophobic property of the hydrophobic part.

In this study, we chose a more hydrophobic monomer; *N*-propargylamide monomer **5** having a longer alkyl chain, i.e., the lauryloyl group, as the hydrophobic part of the amphiphilic copolymer. The monomer **5** was copolymerized with **1** in the presence of Rh catalyst to give the corresponding amphiphilic copolymer **6** (Scheme 2). The resulting copolymer **6** can be expected to have the ability to conduct molecular aggregation in water, which is driven by intermolecular and intramolecular association of the hydrophobic lauryloyl groups.

We believe that such molecular aggregates of the amphiphilic copolymer should play a significant role in the field of targeted drug delivery. The idea is supported by the following characteristics of the molecular aggregates:

1) Drug carriers with nanometer dimensions can be obtained by molecular aggregation of amphiphilic copolymers.
2) Nano-sized aggregates can remain in the bloodstream for an extended period because of the size-dependent uptake in the reticuloendothelial system.
3) Drug molecules with hydrophobic natures can be loaded into hydrophobic milieus formed by the association of hydrophobic long alkyl chains; otherwise the drug molecules could be directly attached to the constituent monomer molecules of the copolymer.
4) Sugar residues of the copolymer can function as recognition sites for target cells and tissues as well as providing the hydrophilic character of the amphiphilic copolymer.

Therefore, we studied the *in vitro* cell uptake of the molecular aggregates of the amphiphilic copolymer. For this purpose, the fluorescent marker, rhodamine B, was introduced into the amphiphilic copolymer. In this article, we report the synthesis of the amphiphilic

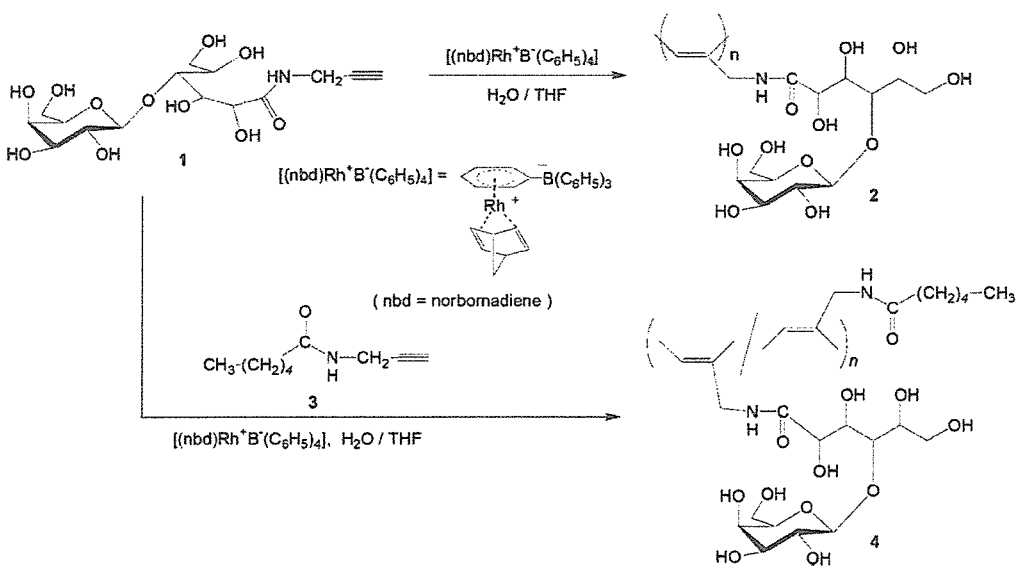

Scheme 1. Polymerization of **1** and copolymerization of **1** with **3**.

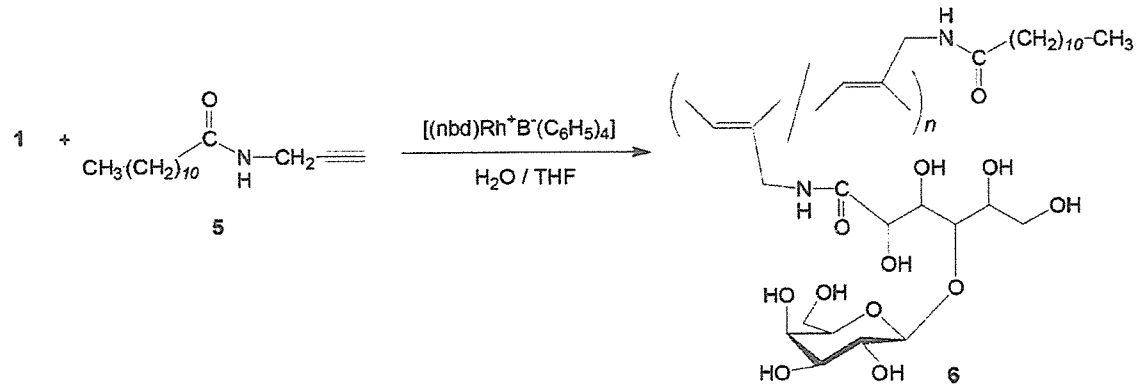

Scheme 2. Copolymerization of **1** with **5**.

poly(*N*-propargylamide) **6** by Rh-catalyzed copolymerization, evaluation of its molecular aggregation in water [gel permeation chromatography (GPC) characterization, scanning electron microscopy (SEM) observation, and dynamic light scattering (DLS) measurement] and secondary conformation [circular dichroism (CD) spectra], and cell uptake of the nanoaggregate of the rhodamine-labeled amphiphilic copolymer (fluorescence microscopy).

Experimental Part

Materials

Monomer **1** and catalyst (nbd)$Rh^+B^-(C_6H_5)_4$ were prepared according to the literature.[12,14] Tetrahydrofuran (THF) used as polymerization solvent was purified by distillation. Other reagents and solvents were used as received without further purification.

Synthesis of Monomer 5

Monomer **5** was synthesized by a method similar to that used for **3**.[15] Under argon, *N*-propargylamine hydrochloride (0.915 g, 10.0 mmol) was dissolved by slight warming in anhydrous acetonitrile (12.0 mL), and triethylamine (3.35 mL, 24.0 mmol) was added to the solution at room temperature. Then a solution of lauryloyl chloride (2.36 mL, 10.0 mmol) in anhydrous acetonitrile (12.0 mL) was added dropwise to the solution. After the mixture was stirred for 2 h, the reaction solution was concentrated by evaporation. The residue was dissolved in ethyl acetate and the solution was washed successively three times with 2 $mol \cdot L^{-1}$ hydrochloric acid and with saturated $NaHCO_3$ aqueous solution. The organic layer was dried over anhydrous Na_2SO_4, filtered, and evaporated. The residue was subjected to column chromatography on silica gel (hexane:ethyl acetate = 4:1, v/v) to isolate **5** (1.38 g, 5.82 mmol) in 58.2% yield.

^{1}H NMR ($CDCl_3$): $\delta = 0.88$ (t, $J = 7.2$ Hz, CH_3, 3H), 1.28 [m, $CH_3(CH_2)_8$, 16H], 1.62 (m, $CH_2CH_2C{=}O$, 2H), 2.19 (t, $J = 7.8$ Hz, $CH_2C{=}O$, 2H), 2.23 (t, $J = 2.4$ Hz, H–C≡C, 1H), 4.05–4.06 (m, CH_2N, 2H), 5.57 (s, NH, 1H).

Synthesis of Monomer 7

Under argon, triethylamine (0.836 mL, 6.00 mmol) was added to a solution of *N*-propargylamine hydrochloride (0.549 g, 6.00 mmol) and rhodamine B (1.92 g, 4.0 mmol) in anhydrous methanol (10.0 mL) at 0 °C. To the solution was added 1-[(3-dimethylamino)propyl]-3-ethylcarbodiimide hydrochloride (1.15 g, 6.00 mmol) as a condensing agent at 0 °C and the mixture was stirred for 17 h at room temperature. The precipitated material was isolated by filtration and dried under the reduced pressure to give **7** (0.472 g, 0.915 mmol) in 23.0% yield.

^{1}H NMR ($CDCl_3$): $\delta = 1.16$ (m, CH_3, 12H), 1.77 (t, $J =$ 2.4 Hz, H–C≡C, 1H), 3.33 (m, NCH_2CH_3, 8H), 3.95 (d, $J = 1.8$ Hz, $CH_2C{\equiv}$, 2H), 6.26–7.93 (m, aromatics, 10H).

Copolymerization of 1 with 5

A typical copolymerization procedure was as follows (entry 1, Table 1). Under argon, a solution of **5** (0.0356 g, 0.150 mmol) in THF (0.90 mL) and a solution of catalyst (0.00630 g, 0.0125 mmol) in THF (0.90 mL) were added to a solution of **1** (0.0397 g, 0.100 mmol) in water (0.20 mL) in this order at 30 °C. After the mixture was stirred at 30 °C for 140 min, the reaction mixture was concentrated by evaporation and dried under reduced pressure. The residue was dissolved in a small amount of DMSO and the solution was poured into a large amount of methanol to precipitate the polymeric product. The precipitate was isolated by filtration and was dried under reduced pressure to give **6** (0.0588 g) in 78.1% yield.

^{1}H NMR (DMSO-d_6): $\delta = 0.84$ (CH_3), 1.21 [$CH_3(CH_2)_8$], 1.45 ($CH_2CH_2C{=}O$), 2.15 ($CH_2C{=}O$), 3.0–3.9 [–CH(O-D-gal)–CH(OH)–CH_2OH, =CCH_2–, H2–H6 of D-gal], 4.04 [C(=O)CH(OH)CH(OH)–], 4.29 [C(=O)CH(OH)– and H1(β) of D-gal], 4.55, 4.79, 5.22 (OH), 6.11 (–CH=C–), 7.93 (NH).

Copolymerization of 1, 5, and 7

Under argon, a solution of **5** (0.0285 g, 0.120 mmol) and **7** (0.0929 g, 0.180 mmol) in THF (0.90 mL) and a solution of catalyst (0.0166 g, 0.0330 mmol) in THF (0.90 mL) were

Table 1. Results for copolymerization of **1** with **5** with Rh catalyst in THF–water (9:1) solvent.

Entry	Feed ratio[a]	Time	Yield[b]	Unit ratio[c]	$\overline{M}_n$[d]	$\overline{M}_w/\overline{M}_n$[d]	$[\alpha]_D$[e]
	1:5	min	%	**1:5**			degrees
1	1.0:1.5	140	78.1	1.0:0.92	9100	1.30	–
2	1.0:1.0	195	62.5	1.0:0.88	6200	1.63	–
3	1.0:0.67	240	57.0	1.0:0.35	5200	1.60	+96.8
4	1.0:0.50	260	68.9	1.0:0.32	9600	1.64	+142.3
5	1.0:0.33	200	69.9	1.0:0.26	7100	1.50	+173.6
6	1.0:0.20	210	78.1	1.0:0.17	9700	1.30	+185.6

[a] [Catalyst]/[**1** + **5**] = 0.05, reaction temperature: 30 °C.
[b] Fraction insoluble in methanol.
[c] Determined from ^{1}H NMR spectra.
[d] Determined by GPC with water as eluent using pullulan standards, sample concentration = 0.1 mg · mL^{-1}.
[e] Measured by polarimetry in water, c = 1.0 g · dL^{-1} at 20 °C.

added to a solution of **1** (0.143 g, 0.360 mmol) in water (0.20 mL) in this order at 30 °C. After the mixture was stirred at 30 °C for 18 h, the reaction mixture was concentrated by evaporation and dried under reduced pressure. The residue was dissolved in a small amount of DMSO and the solution was poured into a large amount of methanol to precipitate the polymeric product. The precipitate was isolated by filtration and dried under reduced pressure to give **8** (0.164 g) in 62.0% yield.

^{1}H NMR (DMSO-d_6 + D_2O): δ = 0.93 ($CH_3CH_2CH_2$), 1.16 (CH_3CH_2N), 1.25 [$CH_3(CH_2)_8$], 1.50 ($CH_2CH_2C{=}O$), 3.0–4.5 (sugar protons and =C–CH_2), 6.16 (HC=), 7.0–8.0 (aromatics).

Cell Culture Experiment

Human aortic endothelial cells (HAECs) were purchased as cryopreserved samples of third passage (Lot: 3F1346) from Cambrex (Wakersville, MD, USA). The HAECs were subcultured once and stored in liquid nitrogen until cell culture experiment. The HAECs used in the experiment were fourth passage. Each well of a 12-well plate of polystyrene (Iwaki) was filled with 1 mL of a supplemented culture medium (EGM-2; Lot: 08103123, Cambrex) and equilibrated at 37 °C in a humidified incubator under 5% CO_2 for 30 min before cell seeding. After the frozen cells were thawed at 37 °C, 10 μL of the cell suspension was seeded in each well. The initial cell density was 2.2×10^3 cells · cm^{-2}. Cell viability assessed by the trypan blue exclusion test was 83% for the cell suspension. The cell seeded plates were placed in a humidified incubator at 37 °C under 5% CO_2. The HAECs were cultured for 48 h. Cell culture mediums were replaced with fresh medium 24 h after cell seeding. At 48 h after cell seeding, cell culture mediums were each replaced with an aqueous suspension of copolymer **8**. Then the HAECs were cultured in the polymer suspension for 1, 6, and 24 h in a humidified incubator at 37 °C under 5% CO_2 to study cellular uptake of nanoaggregates of copolymer **8**. For fluorescence microscopy observation, the cells were fixed by immersion in 10% formaldehyde neutral buffer solution (Nacalai Tesque) at room temperature (22 °C) for 15 min and were washed three times with phosphate-buffered saline (PBS; Gibco). Fluorescence images of the cells were taken with a fluorescence microscope (IX71; Olympus) equipped with a CCD camera (DP70; Olympus). Fluorescence intensity of the incorporated copolymer **8** was measured by integrating the fluorescence intensity observed at each pixel of the fluorescence images using image analysis software (Fluoview ver. 5.0; Olympus).

Measurements

NMR spectra were recorded on a JEOL ECA 600 spectrometer. Optical rotations were measured with a Jasco P-1030 digital polarimeter. GPC analyses were performed by using a TOSOH 8012 with refractive index detection under the following conditions: Shodex Asahipak GF-310HQ column with water as eluent at a flow rate of 0.5 mL · min^{-1}. The calibration curve was obtained using pullulan standards. CD and UV-vis spectra were measured in a quartz cell (thickness 1 cm) at room temperature using a Jasco J-820 spectropolarimeter and Shimadzu UV160A spectrophotometer, respectively. The SEM images were obtained using a Hitachi S-4100 electron microscope. The DLS measurement was performed on a Zetasizer 3000 (Malvern Instruments). Fluorescence spectra were obtained on a fluorescence spectrometer (Shimadzu) using a quartz cuvette (1-mm path length).

Results and Discussion

Copolymerization of 1 with 5

The polymerization of monosubstituted acetylene derivatives has been widely investigated using Rh complex catalysts, which enables stereoselective synthesis of the corresponding polyacetylenes of the *cis*-isomers.[16] As

already reported in our previous publication, **1** was polymerized using (nbd)Rh$^+$B$^-$(C_6H_5)$_4$ as the catalyst at around 25° to 50 °C in a mixed solvent of THF and water (9:1, v/v).[12] In this study, we performed the copolymerization of **1** with **5** under similar conditions. The copolymerization with various feed ratios of **1** to **5** was carried out using the Rh catalyst (5.0 mol-% for **1** + **5**) at 30 °C in a THF-water mixed solvent under argon. After polymerization, the resulting mixture was concentrated and then dissolved in DMSO. The solution was poured into a large amount of methanol to precipitate the polymeric product. The precipitate was isolated by filtration and dried under reduced pressure to give the copolymer **6** (Table 1). The copolymer was soluble in water and DMSO, and its $\overline{M}_n$ value was estimated by GPC analysis with water as eluent using pullulan standards. Figure 1a shows the ^{1}H NMR spectrum of the copolymer (entry 1, Table 1) measured in DMSO-d_6. The signals due to the sugar and alkyl protons are observed at around δ 3.0–4.3 (signals **e–h**) and δ 0.84, 1.21, 1.45, 2.15 (signals **a–d**), respectively. In addition to these signals, signal **i** ascribed to the main-chain proton of –CH=C– appears centered at δ 6.11. The chemical shift of this signal realistically corresponds to the *cis*-isomer. Furthermore, there is no signal due to the *trans*-isomer at lower magnetic field from the *cis*-signal. The NMR results support structure **6** as that of the copolymer, which is mainly composed of *cis*-isomer. The unit ratio of the copolymer is calculated by the integrated ratio of signal **a** and signal **i**.

Table 1 shows the copolymerization results obtained by the various feed ratios of **1** to **5**. The yields and the $\overline{M}_n$ values are 57.0–78.1% and 5 200–9 700, respectively. The unit ratios of **5** in the copolymers increase with increasing molar ratios of **5** in the feeds. In all cases, however, the ratios of **5** in the copolymers are lower than those in the feeds. This is probably because the copolymers with higher

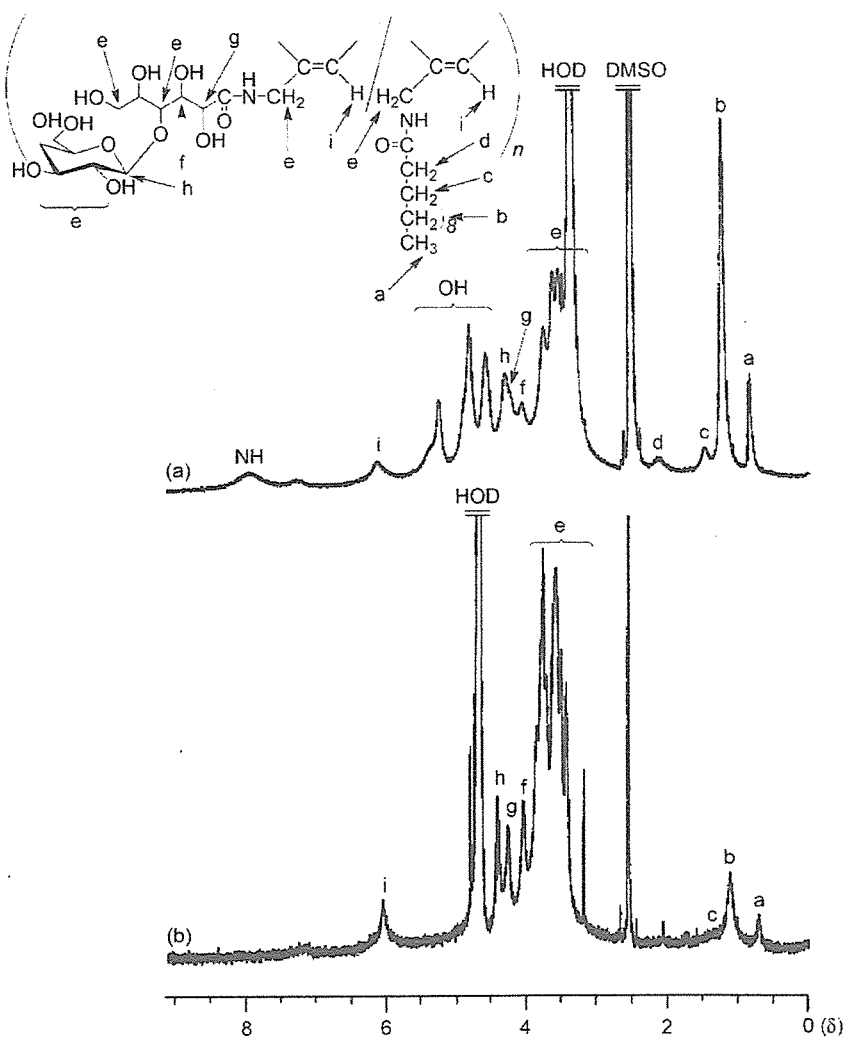

Figure 1. ^{1}H NMR spectra of copolymer **6** (entry 1, Table 1) in DMSO-d_6 (a) and D_2O (b).

contents of the unit **5** are lost as methanol-soluble fractions during the isolation procedure. The optical rotations of the copolymers with the higher contents of the sugar units were larger than those with the lower contents.

Formation of Molecular Aggregates in Water

When the copolymerization was followed by thin-layer chromatography (TLC) on silica gel (methanol: chloroform = 2:1 for **1**; hexane: ethyl acetate = 1: 1 for **5**), **1** appeared to be consumed at the early stage of the reaction; subsequently, the consumption of **3** at a later stage was confirmed. This indicated that **6** had the block copolymeric sequence between the unit **1** and the unit **5** rather than in random style. In fact, the intensities of the alkyl signals **a**–**d** in the ^{1}H NMR spectrum of **6** in D_2O (Figure 1b) are obviously lower than those of the same copolymer measured in DMSO-d_6 (Figure 1a). The NMR results suggest formation of micelle-like aggregates having the outer hydrophilic sugar residues and the inner hydrophobic lauryloyl groups in water, and this was attributed to the block copolymeric sequence. The formation of molecular aggregates of **6** in water was also confirmed by the GPC measurements on aqueous solutions of **6** (entry 5, Table 1, the unit ratio of **1** to **5** = 1.0:0.26) ranging in concentration from 0.05 to 9.0 mg · mL^{-1}. Figure 2 shows the relations of the $\overline{M}_n$ values to the sample concentrations in the GPC experiments. The $\overline{M}_n$ values increase from ca. 6300 to ca. 11000 for concentrations higher than 0.70 mg · mL^{-}. These data suggest the formation of molecular aggregates for the higher concentrations of **6** in water. The molecular aggregates of **6** were directly observed by SEM. The SEM image of the spin-coated sample from the aqueous solution of **6** (entry 4, Table 1, the unit ratio of **1** to **5** = 1.0:0.32) on aluminium plate (Figure 3) shows the particle-type molecular aggregates with average diameters of 20–40 nm. The particle sizes were also confirmed by DLS measurement. The mean particle diameter of the sample shown as entry 4 in Table 1 was 85.2 ± 14.1 nm. The difference in the aggregate sizes obtained by SEM and DLS can be attributed to the difference in the sample condition: dry for SEM and wet for DLS.

Secondary Conformation of 6

We already reported in our previous report that the CD spectrum of the homopolymer **2** in water showed the positive Cotton effect at 330 nm corresponding to the main-chain UV-vis absorption.[12] This indicated the possibility for formation of a one-handed helical conformation in the main chain of **2**. In this study, the CD analysis was also performed to reveal the secondary conformation of copolymer **6**. Figure 4 shows the CD spectra of **6** (entry 5, Table 1, unit ratio of **1** to **5** = 1.0:0.26) in comparison with those of copolymer **4** (unit ratio of **1** to **3** = 1.0: 0.39) measured in DMSO and water at room temperature. The CD spectrum of **6** in DMSO (Figure 4a) shows the positive Cotton effect at 360 nm, corresponding to the main-chain UV-vis absorption. The positive Cotton effect also appeared at this region in the CD spectrum in water (Figure 4b), although its intensity was lower than that in DMSO. It has been reported that the helical structure of poly(*N*-propargylamide)s is stabilized by the intramolecular hydrogen bonds between the pendant amide groups.[17] In polar solvents such as DMSO and water, therefore, the hydrogen bonds are readily broken to effect destabilization of the helical structure. The helical conformation of **6** in polar solvents is probably stabilized by the bulky substituents in the side chains of sugar and lauryloyl groups. These bulky groups shield the hydrogen bonds from the solvents, which consequently stabilizes the helical structure. This reasoning is also supported by comparison of the CD spectra of copolymer **4** (gray lines in

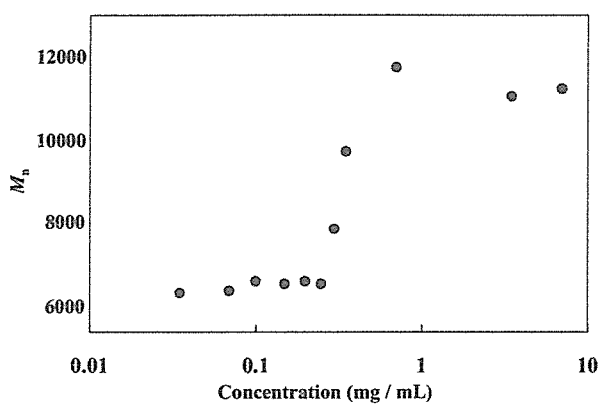

Figure 2. $\overline{M}_n$ values versus sample concentrations in GPC measurements with water as eluent (entry 5, Table 1).

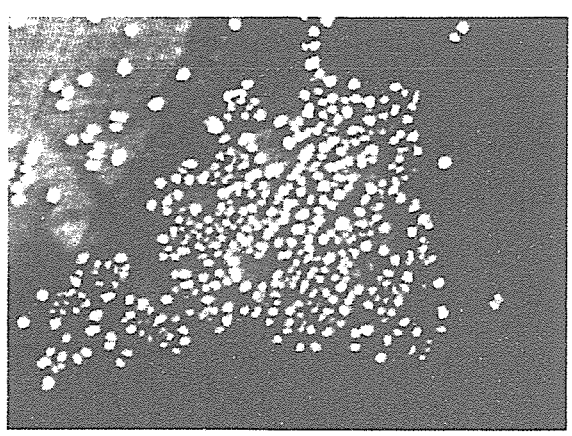

Figure 3. SEM image of **6**; the sample was prepared by spin coating of the dispersed solution of **6** (entry 4, Table 1) in water.

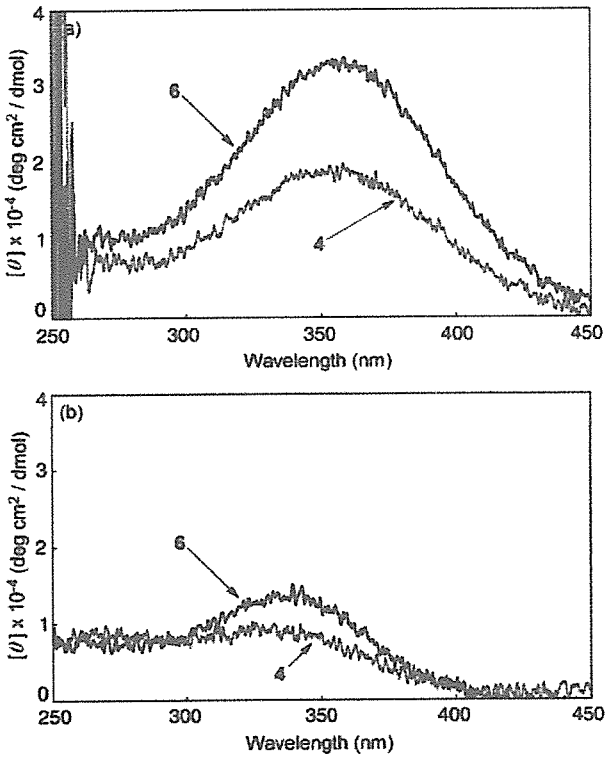

Figure 4. CD spectra of **6** (entry 5, Table 1, unit ratio; **1**:**5** = 1.0:0.26) and **4** (unit ratio; **1**:**3** = 1.0:0.39) in DMSO (a) and water (b) ($c = 0.2$ mmol·L^{-1}).

Figure 4a, b), which has the less bulky hexanoyl groups. The CD spectra of **4** show weaker Cotton effects than those of **6**, indicating the stabilization of the helical conformation as a result of the bulkiness of the pendant groups.

Cellular Uptake of Amphiphilic Copolymer 8

To evaluate cell uptake of the copolymer by fluorescence microscopy, the rhodamine B dye moiety was introduced into the amphiphilic copolymer. First, an *N*-propargylamide derivative **7** having a pendant rhodamine B moiety was prepared by condensation of *N*-propargylamine hydrochloride with rhodamine B in the presence of a condensing agent (1-[(3-dimethylamino)propyl]-3-ethylcarbodiimide hydrochloride) in methanol. Then, the isolated **7** was copolymerized with **1** and **5** under conditions similar to those described above (Scheme 3). Although **7** did not have homopolymerizability by Rh catalyst, the unit from **7** was slightly incorporated into the resulting terpolymer by the copolymerization. The existence of the rhodamine B moiety in the obtained terpolymer **8** was confirmed by appearance of the signals due to methyl protons of N-CH_2CH_3 as well as the aromatic protons in the ^{1}H NMR spectrum of the product. However, the intensities of the signals were too weak to determine the exact content of the dye moiety in the copolymer by the integration ratio. For comparison, hydrophilic copolymer **9** was synthesized by copolymerization of monomer **1** with monomer **7** using Rh catalyst (Figure 5).

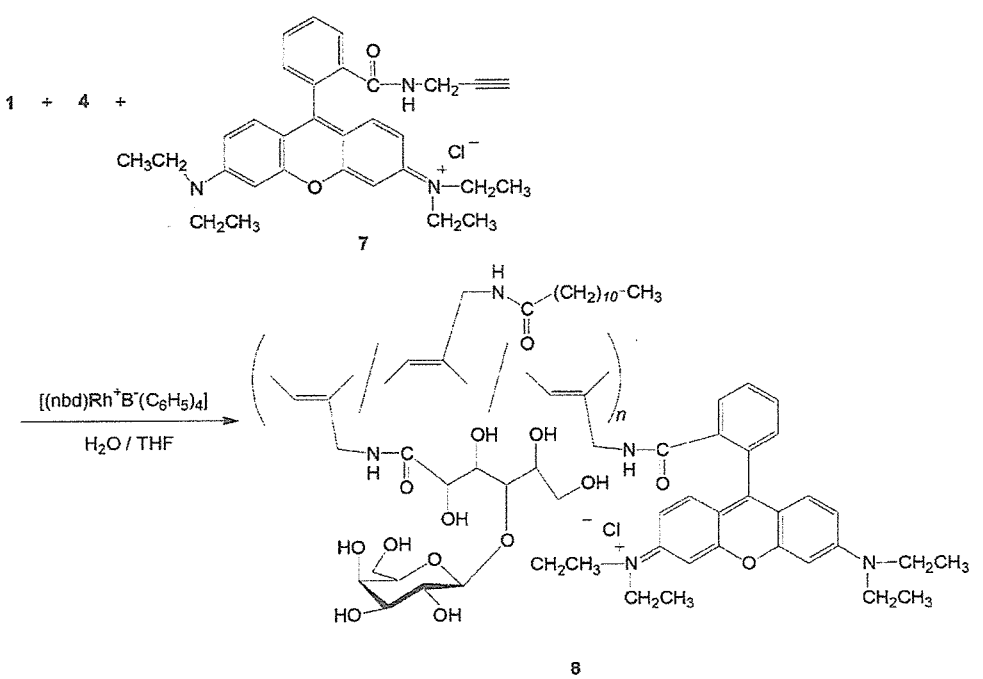

Scheme 3. Terpolymerization of **1**, **5**, and **7**.

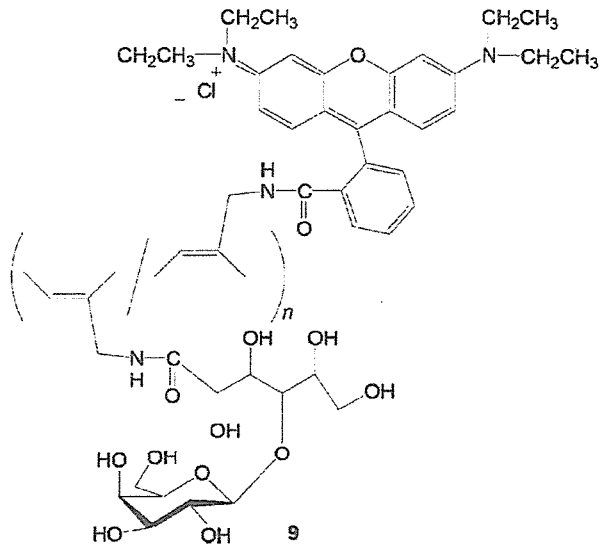

Figure 5. Structure of copolymer **9**.

The cell uptake of terpolymer **8** was studied by culturing human aortic endothelial cells (HAECs) in a culture medium containing the terpolymer **8**. Ten milligrams of **8** was suspended in 10 mL of culture medium EGM-2 and stirred for 3 h at room temperature. The suspension of **8** was sonicated at 25 W and 40 kHz for 5 min in an ultrasonic bath. The sonication was repeated twice. The obtained suspension was filtered through membrane filters with the pore sizes of 0.45 μm and 0.2 μm for sterilization. An aqueous solution of polymer **9** was prepared by following the above procedure. To evaluate the concentration of **8**, a calibration curve (data not shown) was obtained by using the aqueous solution of **9** (1 mg · mL^{-1}) as a standard polymer sample to relate concentration to fluorescence intensity. The concentration of **8** was estimated to be 0.09 mg · mL^{-1} by using the calibration curve. The DLS measurement revealed that the polymer aggregates (nanoparticles) of **8** have a mean diameter of 114.9 ± 32 nm in a culture medium containing 10% bovine serum. HAECs were exposed to the polymer aggregates of **8** while they were cultured in the culture medium containing the amphiphilic polymer **8**. After the prescribed period of culture, 1, 6, or 24 h, the HAECs were fixed in 10% formaldehyde neutral buffer solution for microscope observation. Figure 6 shows phase contrast (a), fluorescence (b), and merged (phase contrast + fluorescence) (c) images of HAECs after 24 h of incubation. The merged image demonstrates that red fluorescent light of rhodamine B was emitted from the sites where HAECs were located. This indicates that the polymer aggregates of **8** were incorporated into HAECs. The fluorescence images at each time of incubation are shown in Figure 7. The fluorescence images get brighter with the incubation time. To quantitatively evaluate cell uptake of nanoaggregates, fluorescence intensity per image (1 360 × 1 024 pixels) was determined by integrating the brightness at each pixel of the fluorescence image using image analysis software. The

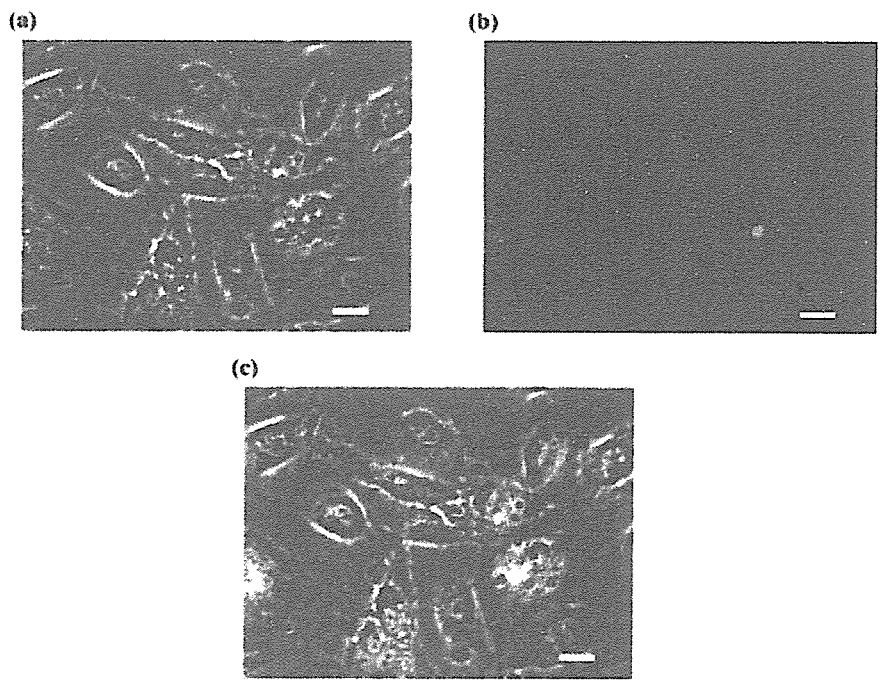

Figure 6a–c. Localization of rhodamine B-labeled copolymer **8** in human aortic endothelial cells. Phase contrast image (a), fluorescence image (b), and merged image of (a) and (b). Bars: 20 μm.

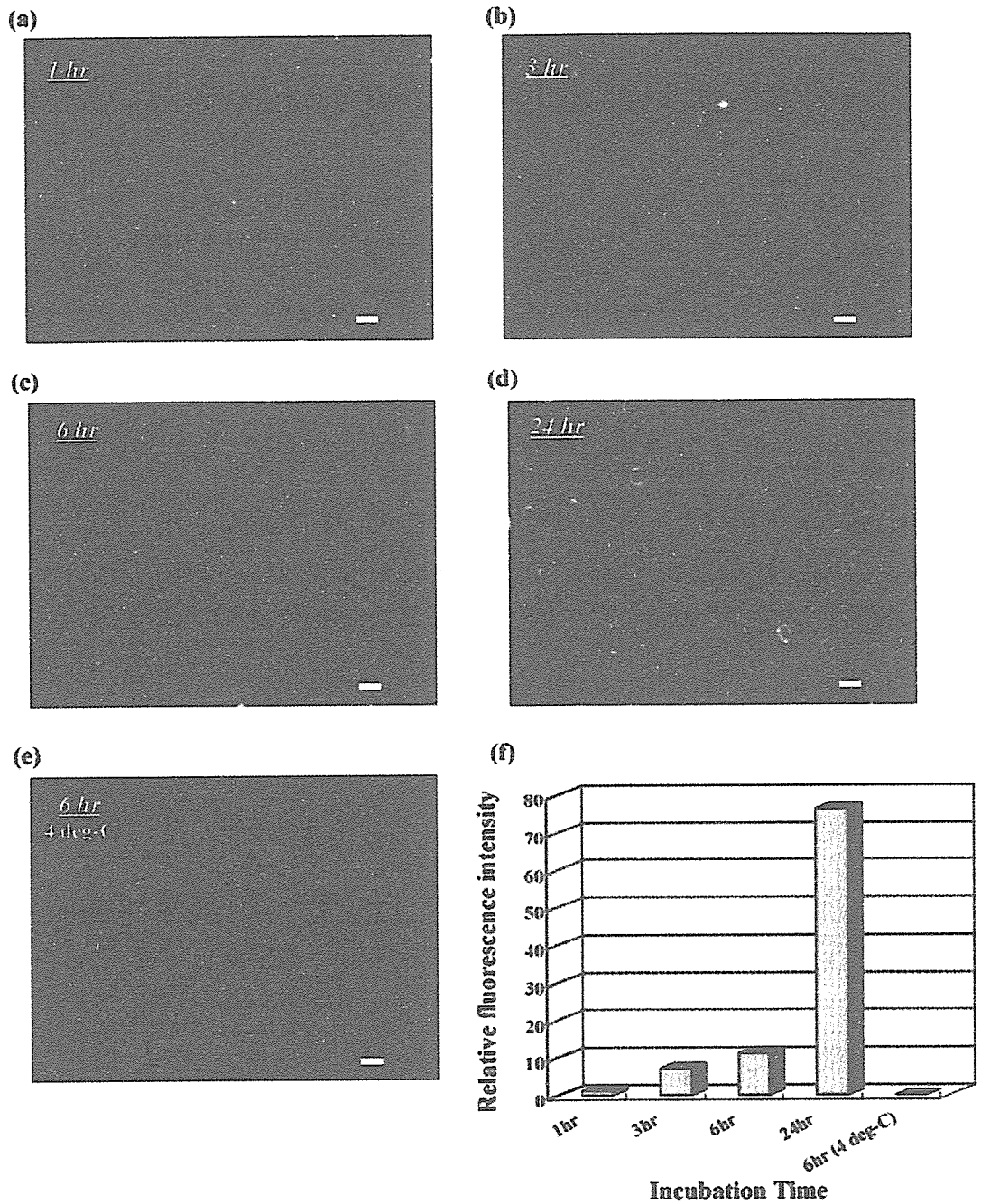

Figure 7a–f. Uptake of rhodamine B-labeled copolymer **8** by human aortic endothelial cells: incubation time, 1 h (a), 3 h (b), 6 h (c), 24 h (d) (incubation at 37 °C), and 6 h (incubation at 4 °C) (e). Bars: 20 μm. The uptake is quantitatively represented as relative fluorescence intensity in the bar graph (f).

fluorescence intensity was normalized in a ratio of the fluorescence intensity at each incubation time to that at 1 h of incubation. The ratio was termed as the relative fluorescence intensity. The time course of the relative fluorescence intensity is shown in Figure 7f and indicates that HAECs incorporated progressively more nanoaggregates of **8** during the incubation time. The relative fluorescence intensity was 7-fold at 3 h, 11-fold at 6 h, and 76-fold at 24 h of incubation. In contrast, the relative fluorescence intensity dropped considerably and was only 12% of the control level (1 h at 37 °C) when HAECs were exposed to the nanoaggregates of **8** at 4 °C for 6 h. The fact that the temperature triggered a dramatic decrease in the relative fluorescence intensity suggests that the nanoag-

gregates are incorporated into HAECs by endocytosis. Endocytosis is known as a cellular process that is coupled with temperature-dependent metabolic activities.[18] Furthermore, it is known that some receptors and membrane microdomains of endothelial cell are involved in endocytosis.[19] However, it is not clear which of the endocytic pathways is responsible for the uptake of the nanoaggregates. This issue is now under investigation.

Conclusion

In this study, we investigated synthesis of the amphiphilic poly(*N*-propargylamide) **6** containing both sugar residues (hydrophilic part) and long alkyl chains (hydrophobic part) in order to develop a novel nanoaggregate based on the self-organization of amphiphilic polymers with rigid backbone. The desired polymer was prepared by copolymerization of the two *N*-propargylamide monomers **1** and **5** having a galactose residue and a lauryloyl group, respectively, catalyzed by a Rh complex. The GPC, ^{1}H NMR, SEM, and DLS analyses of the resulting copolymers indicated formation of the nanoparticles in water. The formation of the one-handed helical conformation of the copolymer in both DMSO and water was confirmed by the CD spectra. An amphiphilic poly(*N*-propargylamide) containing fluorescent dyes was newly designed to evaluate cell uptake of nanoparticles of the amphiphilic copolymer by fluorescence microscopy. The *N*-propargylamide monomer **7**, having a rhodamine B dye moiety, was prepared and copolymerized with **1** and **5**. Human aortic endothelial cells (HAECs) were cultured in a medium containing the fluorescent-dye-labeled amphiphilic copolymer. Cell uptake of the copolymer was confirmed by red fluorescence emission from each of the HAECs. Progressive uptake was observed during the incubation period. When the cell culture experiment was conducted at 4 °C, the fluorescence intensity of the red emission was considerably lowered. This indicates that the cell uptake is inhibited at 4 °C and that this uptake process should occur in an endocytic pathway rather than by simple adsorption to the plasma membrane of HAECs. We are now synthesizing a fluorescent-dye-labeled hydrophilic copolymer of monomer **1** with monomer **7** to study preferential cell uptake of the nanoaggregates of the amphiphilic copolymer. In the future, we anticipate that nanoparticles will be able to be preferentially endocytosed into cells rather than monomeric chains of water-soluble copolymer. If this does occur, the nanoparticles of the amphiphilic copolymer will be a promising nanocarrier for drug delivery.

Acknowledgements: This work was financially supported by the *Asahi Glass Foundation*. The author (T. N.) thanks Professor *Mitsuru Akashi* of Osaka University and Dr. *Takami Akagi* of the Japan Science and Technology Agency for dynamic light scattering measurement. The author (T. N.) thanks Dr. *Tetsuji Yamaoka* and Dr. *Atsushi Mahara* of the National Cardiovascular Center Research Institute for fluorescence spectroscopy analysis.

[1] M. Okada, *Prog. Polym. Sci.* **2001**, *26*, 67.
[2] Y. C. Lee, R. T. Lee, "*Neoglycoconjugates: Preparation and Applications*", Academic Press, San Diego **1994**.
[3] K. Kobayashi, A. Tsuchida, T. Usui, T. Akaike, *Macromolecules* **1997**, *30*, 2016.
[4] K. Kobayashi, N. Kakishita, M. Okada, T. Akaike, T. Usui, *J. Carbohydr. Chem.* **1994**, *13*, 753.
[5] L. L. Kiessling, N. L. Pohl, *Chem. Biol.* **1996**, *3*, 71.
[6] M.-G. Baek, R. C. Stevens, D. H. Charych, *Bioconjugate Chem.* **2000**, *11*, 777.
[7] I.-B. Kim, B. Erdogan, J. N. Wilson, U. H. F. Bunz, *Chem. Eur. J.* **2004**, *10*, 6247.
[8] T. Hasegawa, S. Kondoh, K. Matsuura, K. Kobayashi, *Macromolecules* **1999**, *32*, 6595.
[9] J. Kadokawa, Y. Shinmen, S. Shoda, *Macromol. Rapid Commun.* **2005**, *26*, 103.
[10] A. Takasu, K. Iso, T. Dohmae, T. Hirabayashi, *Biomacromolecules* **2006**, *7*, 411.
[11] K. Matsuura, S. Furuno, K. Kobayashi, *Chem. Lett.* **1998**, 847.
[12] J. Kadokawa, K. Tawa, M. Suenaga, Y. Kaneko, M. Tabata, *J. Macromol. Sci., Pure Appl. Chem.* **2006**, *43*, 1179.
[13] J. Deng, J. Tabei, M. Shiotsuki, F. Sanda, T. Masuda, *Macromolecules* **2004**, *37*, 9715 and references therein.
[14] R. R. Shrock, J. A. Osborn, *Inorg. Chem.* **1970**, *9*, 2339.
[15] J. Deng, J. Tabei, M. Shiotsuki, F. Sanda, T. Masuda, *Macromolecules* **2004**, *37*, 1891.
[16] M. Tabata, T. Sone, Y. Sadahiro, *Macromol. Chem. Phys.* **1999**, *200*, 265.
[17] J. Tabei, R. Nomura, T. Masuda, *Macromolecules* **2002**, *35*, 5405.
[18] G. Durin, S. Cottin, E. Blanc, A. R. Rees, *J. Temsamani, J. Biol. Chem.* **2003**, *278*, 31192.
[19] S. Muro, M. Koval, V. Muzykantov, *Curr. Vasc. Pharmacol.* **2004**, *2*, 281.

